



# HO<sub>2</sub>NO<sub>2</sub> and HNO<sub>3</sub> in the coastal Antarctic winter night: a “lab-in-the-field” experiment

A. E. Jones<sup>1</sup>, N. Brough<sup>1</sup>, P. S. Anderson<sup>1,\*</sup>, and E. W. Wolff<sup>1,\*\*</sup>

<sup>1</sup>British Antarctic Survey, Natural Environment Research Council, Cambridge, UK

\* now at: Scottish Association of Marine Science, Scottish Marine Institute, Oban, UK

\*\* now at: Dept of Earth Sciences, University of Cambridge, Cambridge, UK

Correspondence to: A. E. Jones (aejo@bas.ac.uk)

Received: 1 May 2014 – Published in Atmos. Chem. Phys. Discuss.: 20 May 2014

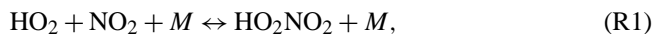
Revised: 12 September 2014 – Accepted: 6 October 2014 – Published: 12 November 2014

**Abstract.** Observations of peroxyntic acid (HO<sub>2</sub>NO<sub>2</sub>) and nitric acid (HNO<sub>3</sub>) were made during a 4 month period of Antarctic winter darkness at the coastal Antarctic research station, Halley. Mixing ratios of HNO<sub>3</sub> ranged from instrumental detection limits to ~8 parts per trillion by volume (pptv), and of HO<sub>2</sub>NO<sub>2</sub> from detection limits to ~5 pptv; the average ratio of HNO<sub>3</sub> : HO<sub>2</sub>NO<sub>2</sub> was 2.0(±0.6) : 1, with HNO<sub>3</sub> always present at greater mixing ratios than HO<sub>2</sub>NO<sub>2</sub> during the winter darkness. An extremely strong association existed for the entire measurement period between mixing ratios of the respective trace gases and temperature: for HO<sub>2</sub>NO<sub>2</sub>,  $R^2 = 0.72$ , and for HNO<sub>3</sub>,  $R^2 = 0.70$ . We focus on three cases with considerable variation in temperature, where wind speeds were low and constant, such that, with the lack of photochemistry, changes in mixing ratio were likely to be driven by physical mechanisms alone. We derived enthalpies of adsorption ( $\Delta H_{\text{ads}}$ ) for these three cases. The average  $\Delta H_{\text{ads}}$  for HNO<sub>3</sub> was  $-42 \pm 2 \text{ kJ mol}^{-1}$  and for HO<sub>2</sub>NO<sub>2</sub> was  $-56 \pm 1 \text{ kJ mol}^{-1}$ ; these values are extremely close to those derived in laboratory studies. This exercise demonstrates (i) that adsorption to/desorption from the snow pack should be taken into account when addressing budgets of boundary layer HO<sub>2</sub>NO<sub>2</sub> and HNO<sub>3</sub> at any snow-covered site, and (ii) that Antarctic winter can be used as a natural “laboratory in the field” for testing data on physical exchange mechanisms.

## 1 Introduction

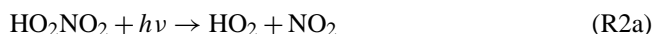
Peroxyntic acid (HO<sub>2</sub>NO<sub>2</sub>, also written as HNO<sub>4</sub>) and nitric acid (HNO<sub>3</sub>) are acidic gases that are of increasing interest to polar tropospheric chemistry. Their primary relevance is that they act as reservoir species for HO<sub>x</sub> and NO<sub>x</sub>, which are now recognised to drive the surprisingly vigorous oxidation chemistry that has been observed during Antarctic summer (e.g. Davis et al., 2001; Chen et al., 2001). The spatial and temporal distribution of HO<sub>2</sub>NO<sub>2</sub> and HNO<sub>3</sub> across the polar regions thus becomes important for understanding the overall atmospheric chemical system, and models require details of their sources, and any physical exchange process by which they move from one environmental compartment to another. Currently, many of these details are unknown.

The gas-phase chemistry of HO<sub>2</sub>NO<sub>2</sub> and HNO<sub>3</sub> is relatively straightforward. Peroxyntic acid is a somewhat unstable molecule that forms and dissociates through its temperature-dependent equilibrium reaction:

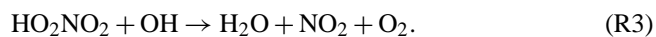


which renders an increased stability for HO<sub>2</sub>NO<sub>2</sub> at lower temperatures.

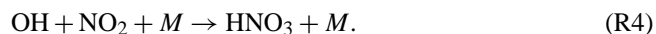
There are a number of photodissociation pathways which drive HO<sub>2</sub>NO<sub>2</sub> and HNO<sub>3</sub> chemistry under sunlit conditions. The most important are thought to be



Peroxyntic acid can also be lost through reaction with OH:



Gas-phase production of nitric acid proceeds via



The major loss processes are reaction with OH and photolysis:



Both HO<sub>2</sub>NO<sub>2</sub> (Ulrich et al., 2012) and HNO<sub>3</sub> (Bartels-Rausch et al., 2002; Hudson et al., 2002; Ullerstam et al., 2005) have been shown in laboratory experiments to adsorb to ice surfaces. This conclusion is supported by field observations which have confirmed uptake of both HNO<sub>3</sub> and HO<sub>2</sub>NO<sub>2</sub> to snow surfaces (Huey et al., 2004; Slusher et al., 2002), and of HNO<sub>3</sub> to cirrus clouds (Weinheimer et al., 1998; Popp et al., 2004; Ziereis et al., 2004). In general, therefore, in snow covered areas, or indeed regions of the atmosphere with lofted snow/ice, such as cirrus clouds or blowing/precipitating snow, physical adsorption of HNO<sub>3</sub> and HO<sub>2</sub>NO<sub>2</sub> from the air to the snow/ice is likely to occur. The details of this uptake will differ somewhat between the two molecules because the partitioning coefficient of HNO<sub>3</sub> is greater than that for HO<sub>2</sub>NO<sub>2</sub>. HNO<sub>3</sub> is thus more sticky than HO<sub>2</sub>NO<sub>2</sub>, and a higher fraction of HNO<sub>3</sub> can be expected on the ice surface compared with HO<sub>2</sub>NO<sub>2</sub>.

High resolution observations of HNO<sub>3</sub> and HO<sub>2</sub>NO<sub>2</sub> in the polar regions are scarce. Critically, both HO<sub>2</sub>NO<sub>2</sub> and HNO<sub>3</sub> have been measured together during a number of Antarctic studies at high temporal resolution. These studies have included both ground-based experiments at the South Pole (Slusher et al., 2002; Huey et al., 2004) and airborne measurements across the wider Antarctic Plateau (Slusher et al., 2010).

The ground-based studies have revealed considerable inter-annual variability in summertime HNO<sub>3</sub> and HO<sub>2</sub>NO<sub>2</sub> mixing ratios, but always of the order of 10 s of pptv at the South Pole. For example, the median observed HNO<sub>3</sub> between 16 and 31 December 2000 was 18.2 pptv and for HO<sub>2</sub>NO<sub>2</sub> was 23.5 pptv (Davis et al., 2004); over the equivalent time period in 2003, the median HNO<sub>3</sub> was 84 pptv, and for HO<sub>2</sub>NO<sub>2</sub> was 39 pptv (Eisele et al., 2008). Considerably greater mixing ratios have also been observed; for example, the median mixing ratio of HNO<sub>3</sub> between 15 and 30 November 2003 was 194 pptv, and of HO<sub>2</sub>NO<sub>2</sub> was 63 pptv (Eisele et al., 2008). While the specific mixing ratios will be strongly influenced by boundary layer height, overall, these high mixing ratios are fuelled by in situ production from elevated levels of NO<sub>x</sub> and HO<sub>x</sub> within the South Pole boundary layer, in turn driven by photochemical release of trace gases from the surrounding snowpack (Davis et al., 2001, 2008).

The airborne measurements assessed the three-dimensional distribution of HO<sub>2</sub>NO<sub>2</sub> and HNO<sub>3</sub> across

the Antarctic Plateau during the ANTCI 2005 campaign (Slusher et al., 2010). They revealed significant vertical gradients in both species, with higher concentrations at the ground, consistent with a source associated with emissions from the snowpack. The measurements also showed a widespread distribution of both HNO<sub>3</sub> and HO<sub>2</sub>NO<sub>2</sub> across the Plateau region.

To date there have been no measurements of high temporal resolution HO<sub>2</sub>NO<sub>2</sub> and HNO<sub>3</sub> in coastal Antarctica, and no measurements at all from Antarctica outside the summer season. We report here observations of HO<sub>2</sub>NO<sub>2</sub> and HNO<sub>3</sub> made using a chemical ionisation mass spectrometer (CIMS) at Halley research station in coastal Antarctica (75°35' S, 26°39' W) from 24 May to 18 September 2007. The data allow us to assess whether HNO<sub>3</sub> and HO<sub>2</sub>NO<sub>2</sub> are present in significant concentrations at other Antarctic locations and seasons than the Antarctic Plateau in summer. They also provide an opportunity to test laboratory-derived physical exchange parameters under semi-constrained, but genuine real-world conditions. At Halley, the sun remains below the horizon from 30 April to 13 August, such that this new data set includes many weeks of winter darkness. Under these conditions of 24 h per day darkness, atmospheric photochemistry stalls, and trace gas concentrations are controlled entirely by either transport or physical air–snow exchange.

## 2 Experimental

### 2.1 CIMS instrumentation

The CIMS instrument used in this study has been described in detail elsewhere (Buys et al., 2013). It was installed in the Clean Air Sector Laboratory (CASLab), which is located roughly 1 km from the main Halley station, and in a sector that rarely receives air from the base (Jones et al., 2008). The CIMS inlet extended ~20 cm above the roof of CASLab, at a height roughly 5 m above the surrounding snowpack. The inlet system was designed to minimise residence time and surface losses (Neuman et al., 1999).

The instrument employed the SF<sub>6</sub><sup>-</sup> method to detect both HNO<sub>3</sub> and HO<sub>2</sub>NO<sub>2</sub>, using the NO<sub>4</sub><sup>-</sup> (HF) cluster at *m/z* 98 to detect HO<sub>2</sub>NO<sub>2</sub>, and NO<sub>3</sub><sup>-</sup> (HF) at *m/z* 82 to detect HNO<sub>3</sub> (as per Slusher et al., 2001, 2002). Calibration was achieved using the SO<sub>2</sub> method as described by Slusher et al. (2001) and Kim et al. (2007). Background measurements, or zeros, were obtained every 10 min. These were achieved by passing sampled air for 3 min through a customised filter filled with activated coarse charcoal and nylon glass wool coated in NaHCO<sub>3</sub>. This scrubbing method has previously been shown to be efficient at removing both HO<sub>2</sub>NO<sub>2</sub> and HNO<sub>3</sub> from sampled air (Slusher et al., 2001). The instrument detection limit derived from background data averaged over 10 min was 0.7 pptv for HNO<sub>3</sub> and 0.4 pptv for HO<sub>2</sub>NO<sub>2</sub>. Total estimated uncertainty in the CIMS observations is ±40 %.

While the SF<sub>6</sub><sup>-</sup> method has been used successfully in previous field campaigns (e.g. Slusher et al., 2002, 2010), it has been demonstrated in laboratory studies (Slusher et al., 2001) that SF<sub>6</sub><sup>-</sup> reacts with H<sub>2</sub>O in the sample air flow. This introduces an interferent into the technique, the non-linearity of which is evident in the unfiltered data (not shown). However, with their instrument reaction time of ~25 ms, Slusher et al. (2001) also concluded that this interferent was significant only at dew points greater than -25 °C, and that at lower dew points, the interferent was negligible. During the period of measurements at Halley, the CIMS instrument also operated with a reaction time of ~25 ms, such that the interferent would be equivalent to that of Slusher et al. (2001). At Halley, dewpoint temperatures varied from -12 to -52 °C (mean -31 °C), but were below -25 °C for 81 % of the time. To remove the potential for H<sub>2</sub>O interference in our data, all measurements made at dew points above -25 °C are filtered out from the data set.

## 2.2 Boundary layer meteorology

Measurements of near-surface boundary layer meteorology were made on a 32 m profiling mast located ~25 m from the CASLab. Bulk sensors were located at 1, 2, 4, 8, 16, and 32 m above ground level, recording at 1 Hz and averaged to 10 min means; temperatures and humidity were measured with platinum resistance thermometers (0.1 K resolution) and solid state humidity probes (2 % resolution), respectively, using an aspirated HMP35D from Vaisala Corp. 10 min vector average wind speed and direction were measured with R. M. Young propeller vanes at 0.1 ms<sup>-1</sup> and 2° resolution.

Three three-axis Metek USA-1 ultrasonic anemometer/thermometers were deployed at the 4, 16, and 32 m levels, sampling at 20 Hz. The data were tilt corrected and the relevant co-variances calculated over 1 min means.

## 3 Results and discussion

### 3.1 Overall data series

The time series of filtered HO<sub>2</sub>NO<sub>2</sub> and HNO<sub>3</sub> data, averaged to hourly means, is shown in Fig. 1, together with hourly means of ambient temperature, dew point temperature, and solar zenith angle. The solar zenith angle shows that the sun was below the horizon for the majority of this time period, and observations of NO and NO<sub>2</sub> (made using a Sonoma Tech. Dual channel chemiluminescence analyser (Bauguitte et al., 2012; Cotter et al., 2003), with detection limits of 2 pptv for NO and 6 pptv for NO<sub>2</sub>, not shown) were consistently below the instrumental detection limits.

Regardless of this apparent lack of photochemical activity, there is considerable variability in the HNO<sub>3</sub> and HO<sub>2</sub>NO<sub>2</sub> observations. Mixing ratios of HNO<sub>3</sub> ranged from instrumental detection limits to ~8 parts per trillion by volume (pptv) and of HO<sub>2</sub>NO<sub>2</sub> varied from detection limits to

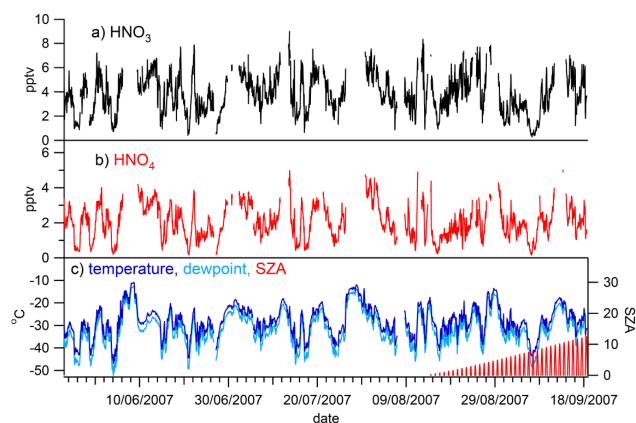


**Figure 1.** Time series of (a) HNO<sub>3</sub>, (b) HO<sub>2</sub>NO<sub>2</sub>, and (c) ambient temperature, dewpoint, and solar zenith angle (SZ) (hourly averages) for the entire measurement period discussed in this paper, 24 May to 18 September 2007.

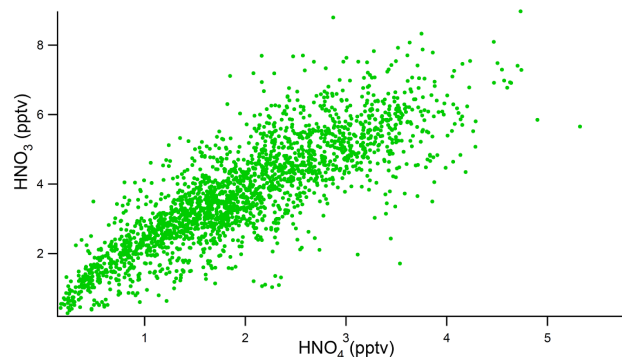


**Figure 2.** Nitric acid (HNO<sub>3</sub>) vs. peroxyntic acid (HO<sub>2</sub>NO<sub>2</sub>); hourly averages of measurements made from 24 May to 18 September 2007.

~5 pptv. These values are considerably lower than those observed at the South Pole in summer, where photochemical production is fuelled by emissions of NO<sub>x</sub> from the snowpack, and where mixing ratios of HNO<sub>3</sub> and HO<sub>2</sub>NO<sub>2</sub> were generally in the 10 s of pptv, and sometimes over 100 pptv, as discussed earlier.

It is also noticeable in the Halley data that the pattern of variability in both HO<sub>2</sub>NO<sub>2</sub> and HNO<sub>3</sub> was very similar, with each time series tracking the other closely. Indeed the correlation between the two chemical species was high, as shown in Fig. 2, where the correlation coefficient,  $R^2$ , for the hourly averages was 0.70. This finding is consistent with the data of Slusher et al. (2002), which showed that, although the range of mixing ratios at the South Pole in summer were considerably higher than observed at Halley during the winter (<5 to 54 pptv for HO<sub>2</sub>NO<sub>2</sub>, and <5 to 68 pptv for HNO<sub>3</sub>), the variability observed in both species during the measurement period was, again, highly coupled.

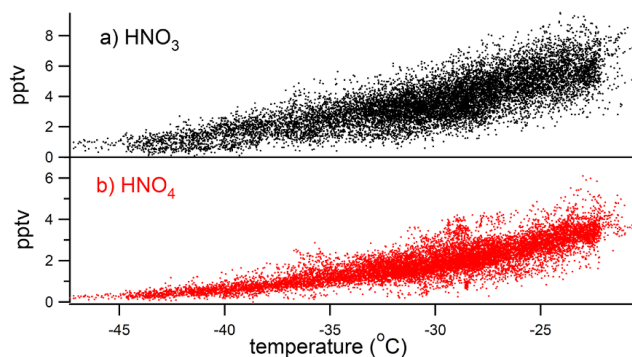


**Figure 3.** (a) Nitric acid (HNO<sub>3</sub>) and (b) peroxyxynitric acid (HO<sub>2</sub>NO<sub>2</sub>) vs. ambient temperature; 10 min averages of measurements made from 24 May to 18 September 2007.

The time series presented in Fig. 1 also clearly shows the very strong association between mixing ratios of HNO<sub>3</sub> and HO<sub>2</sub>NO<sub>2</sub> and ambient (and dewpoint) temperature. This association is further demonstrated in Fig. 3, which shows both HNO<sub>3</sub> and HO<sub>2</sub>NO<sub>2</sub> plotted against ambient temperature, again for the entire period of measurements. Calculated correlation coefficients with temperature are high, with  $R^2 = 0.70$  and  $0.72$  for HNO<sub>3</sub> and HO<sub>2</sub>NO<sub>2</sub> respectively.

Given that mixing ratios of HNO<sub>3</sub> and HO<sub>2</sub>NO<sub>2</sub> are so strongly associated with ambient temperature, Table 1 gives the mean and standard deviation of HNO<sub>3</sub> and HO<sub>2</sub>NO<sub>2</sub> measured between 24 May and 18 September 2007, calculated within specific temperature ranges. The statistics are derived using only the filtered data that were above  $3\sigma$  detection limits. At the South Pole during the summer, ambient temperature ranged from  $-31.5$  to  $-23.6$  °C, with a mean of  $-27.7$  °C; within this temperature range, HNO<sub>3</sub> mixing ratios ranged from  $< 5$  to 54 pptv (mean 25 pptv) and HO<sub>2</sub>NO<sub>2</sub> ranged from  $< 5$  to 68 pptv (mean 22 pptv). For the equivalent temperature range at Halley (also with a mean of  $-27.7$  °C), mean and maximum mixing ratios for HNO<sub>3</sub> were 4.4 and 9 pptv respectively, and for HO<sub>2</sub>NO<sub>2</sub> were 2.5 and 5 pptv respectively, clearly significantly below those observed at the South Pole, for the reasons outlined above.

Differences between South Pole summer and Halley winter are also evident in the ratio of HNO<sub>3</sub>:HO<sub>2</sub>NO<sub>2</sub>, arising through differences in the species' lifetimes. Throughout the Halley measurement period, the average ratio of HNO<sub>3</sub>:HO<sub>2</sub>NO<sub>2</sub> was  $2.0(\pm 0.6):1$ , with HNO<sub>3</sub> always (apart from a few outliers) present at greater mixing ratios than HO<sub>2</sub>NO<sub>2</sub> during the winter darkness (see Fig. 4). This finding is in contrast to observations from the South Pole during sunlit summer time, when mixing ratios of HNO<sub>3</sub> and HO<sub>2</sub>NO<sub>2</sub> were roughly equal for much of the measurement period (Slusher et al., 2002). Figure 1 of Slusher et al. (2002) shows that HO<sub>2</sub>NO<sub>2</sub> was present at higher mixing ratios than HNO<sub>3</sub> for roughly 2 out of the 7 days of measurements; during the roughly 4 months of measurements at Halley, the only

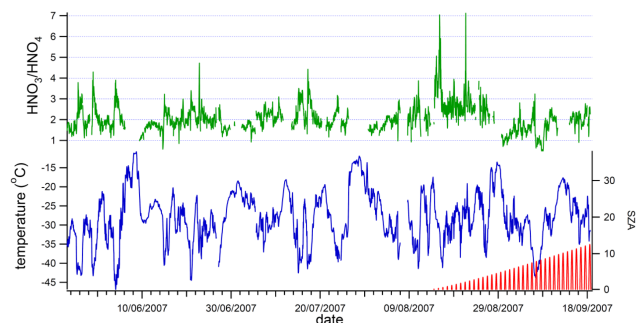


**Figure 4.** Ratio of HNO<sub>3</sub>:HO<sub>2</sub>NO<sub>2</sub> (hourly average data) for the May to September measurement period. Also shown, for reference, are ambient temperature and solar zenith angle.

occasion when the mixing ratio of HO<sub>2</sub>NO<sub>2</sub> exceeded that of HNO<sub>3</sub> was on the 6 and 7 September, a period when temperatures were particularly low but there was a limited amount of sunlight.

### 3.2 Short-term variability in HNO<sub>3</sub> and HO<sub>2</sub>NO<sub>2</sub> and link to ambient temperature

The short-term variability in the HNO<sub>3</sub> and HO<sub>2</sub>NO<sub>2</sub> is shown more clearly in Fig. 5. The three examples show periods when ambient air temperatures varied rapidly and considerably, but where they remained below the  $-25$  °C dewpoint threshold such that no chemical data filtering was required. These 10 min averages show that even very small-scale features of temperature change are reflected in the chemical measurements. For example, at midnight on 5 June, the short-lived peak in temperature is reflected also in HNO<sub>3</sub> and HO<sub>2</sub>NO<sub>2</sub>; the temperature peak around 11 a.m. on 21 June is apparent with similar, small, peaks in HNO<sub>3</sub> and HO<sub>2</sub>NO<sub>2</sub>; and the short-lived temperature peak around noon on 15 July is also evident in short-lived increases in HNO<sub>3</sub> and HO<sub>2</sub>NO<sub>2</sub> mixing ratios. While large-scale variability in HNO<sub>3</sub> and HO<sub>2</sub>NO<sub>2</sub> could be linked to air mass origin, such fine-scale variability can only be explained by a local, fast-acting, source/sink mechanism. The association between variability in HNO<sub>3</sub> and HO<sub>2</sub>NO<sub>2</sub> and changes in ambient temperature strongly suggest a temperature-dependent mechanism. Given our understanding of the interaction between acidic gases and ice gained through laboratory studies (e.g. Huthwelker et al., 2006), one possible mechanism is temperature-dependent adsorption/desorption at the snow surface.

### 3.3 Evidence for HO<sub>2</sub>NO<sub>2</sub> and HNO<sub>3</sub> air/snow exchange

To probe in more detail the response of HNO<sub>3</sub> and HO<sub>2</sub>NO<sub>2</sub> to changes in temperature, we examined periods in the data where ambient temperatures changed, but where wind speeds were relatively low and invariable. By adopting this ap-

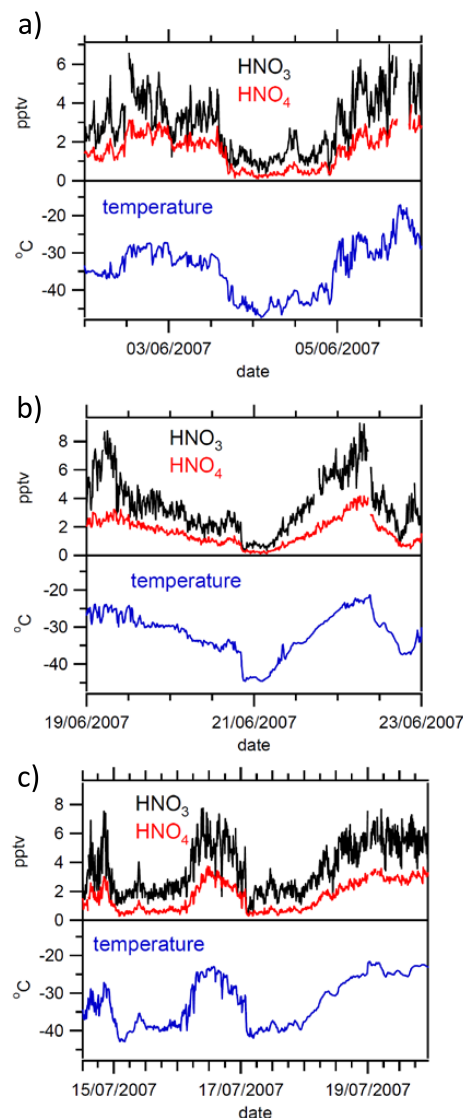
**Table 1.** Mean and standard deviation of nitric acid and peroxyntic acid according to ambient air temperature range. The statistics were derived using only data above the 3 $\sigma$  detection limit.

Ambient air temperature (°C)	Nitric acid			Peroxyntic acid		
	no. points	mean (pptv)	SD (pptv)	no. points	mean (pptv)	SD (pptv)
−45 to −47.4	24	0.96	0.12	0		
−40 to −45.9	579	1.36	0.42	472	0.58	0.14
−35 to −39.9	1575	2.13	0.74	1615	0.99	0.38
−30 to −34.9	3638	3.09	0.92	3732	1.6	0.44
−25 to −29.9	4821	4.32	1.18	4942	2.29	0.62
−21.2 to −24.9	1954	5.67	1.19	2013	3.23	0.62

proach, we minimise any influence that air flow through the snow (e.g. via ventilation/wind pumping) may have on air/snow exchange processes. We derive a mixing diffusivity to determine the timescale for vertical mixing (via turbulent diffusion) between the snow surface and the CIMS inlet height, in order to confirm that the CIMS HNO<sub>3</sub> and HO<sub>2</sub>NO<sub>2</sub> observations can be used to analyse processes occurring at the ground-level air/snow interface. The mixing diffusivity is roughly equal to  $kz u_*$ , where  $k$  is von Karman's constant (0.4),  $z$  is CIMS inlet height (5 m) and  $u_*$  is the friction velocity, derived from the sonic anemometer data (Stull, 1988). The  $e$ -folding time scale,  $t_{sc}$ , is given by  $z^2/\text{diffusivity}$ , that is  $t_{sc} = z/(k u_*)$ . During each case study  $t_{sc}$  will vary, but cannot be negative: this range is presented below derived from log means and standard deviations. Figure 6a shows observations made on 30 May 2007, with a clear gradual increase in both HNO<sub>3</sub> and HO<sub>2</sub>NO<sub>2</sub> as ambient temperatures rose from  $\sim -44$  to  $\sim -30$  °C. On this day, data from the boundary layer mast (not shown) show that between the surface and 8 m height, there was little or no temperature gradient; to first order, therefore, 8 m temperatures can be used as a surrogate for those at the ground. Wind speeds were between 0 and 2 m s<sup>−1</sup> from the surface to 4 m, and remained at around 2 m s<sup>−1</sup> at 8 m height. For 95 % of the time,  $t_{sc}$  was between 100 and 300 s.

Figure 6b shows data for the period from 9 a.m. to midnight on 21 June, discussed briefly in Sect. 3.2 above. Again, a gradual increase in mixing ratios of HNO<sub>3</sub> and HO<sub>2</sub>NO<sub>2</sub> is evident (upper panel), as ambient temperatures rose gradually from  $\sim -38$  to  $\sim -26$  °C. Data from the boundary layer met mast show that, during this period, there was no vertical gradient in temperature between the surface and 8 m height; wind speeds from the surface to 8 m were below 2 m s<sup>−1</sup>. Data from the sonic anemometers show that vertical mixing was again very weak, with mixing time scales between 90 and 600 s.

Figure 6c shows observations from midnight to 9 a.m. on 18 July, another quiescent period, with wind speeds in the lowest 8 m below 1 m s<sup>−1</sup>, and with no temperature gradient below 32 m. Gradual increases in both HNO<sub>3</sub> and HO<sub>2</sub>NO<sub>2</sub>

**Figure 5.** Three examples of short-term variability in HNO<sub>3</sub>, HO<sub>2</sub>NO<sub>2</sub> and ambient air temperature (10 min data), from (a) early June; (b) mid June; and (c) mid July. All three periods are during the winter 24 h per day darkness.

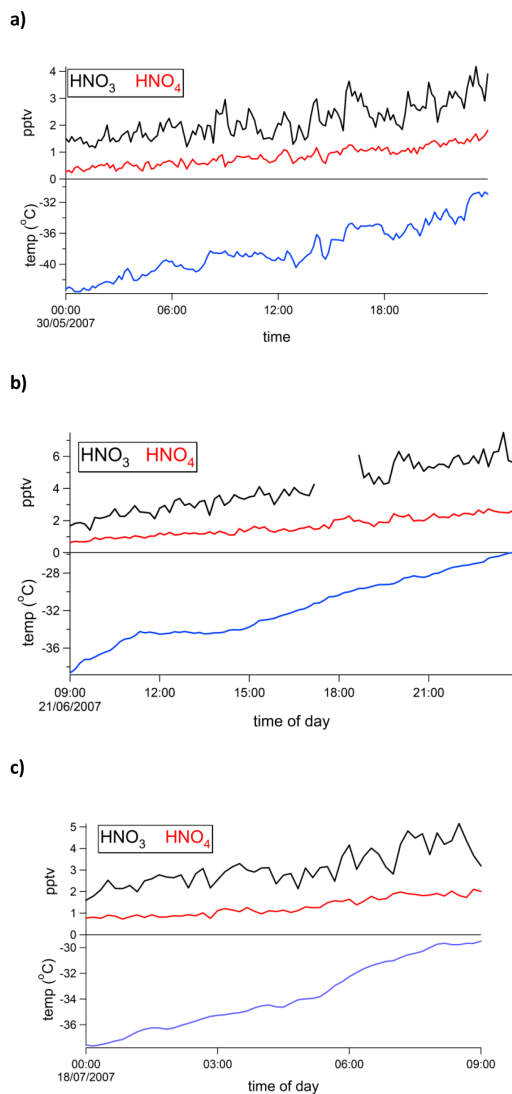


**Figure 6.** Detail of changes in HNO<sub>3</sub>, HO<sub>2</sub>NO<sub>2</sub> and temperature on (a) 30 May, (b) 21 June, and (c) 18 July. These three periods in the measurement series were characterised by low and invariant wind speeds and 24 h per day darkness.

proceed as ambient temperatures rise from  $-38$  to  $-30$  °C.  $t_{sc}$  varied between 30 and 100 s during the event.

Correlation coefficients between mixing ratios of HNO<sub>3</sub> (and HO<sub>2</sub>NO<sub>2</sub>) and temperature, are extremely high for the time periods presented in Fig. 6:  $R^2$  for the correlation between HNO<sub>3</sub> and temperature is 0.72 (30 May), 0.90 (21 June) and 0.72 (18 July); for the correlation between HO<sub>2</sub>NO<sub>2</sub> and temperature,  $R^2$  was 0.88 (30 May), 0.94 (21 June), and 0.92 (18 July). The values of  $R^2$  show that between 72 and 90 % of the variability in HNO<sub>3</sub> can be explained by variability in temperature; and between 88 and 94 % of the variability in HO<sub>2</sub>NO<sub>2</sub> can be explained by the variability in temperature.

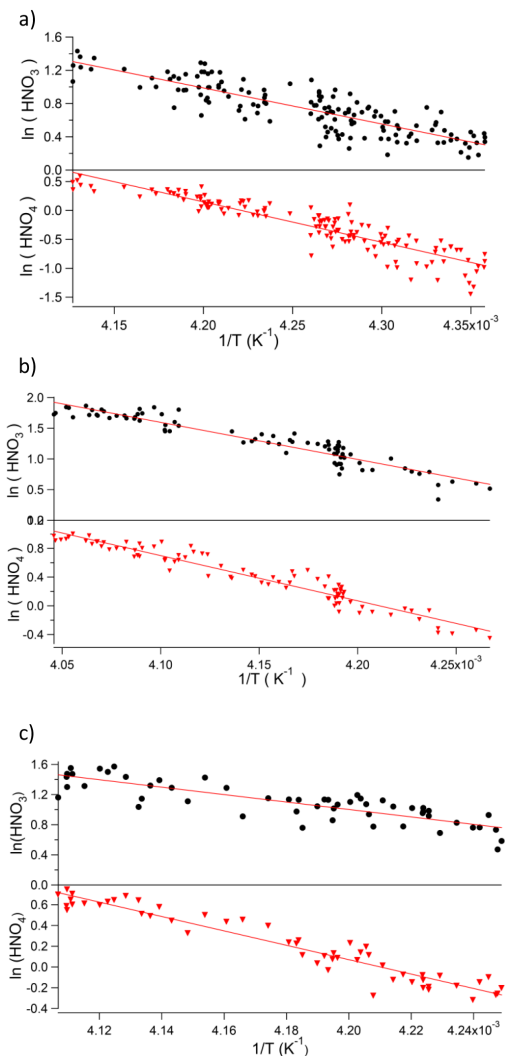


**Figure 7.** Plots of  $\ln(\text{HNO}_3)$  and  $\ln(\text{HO}_2\text{NO}_2)$  vs.  $1/T$  for the time periods shown in Fig. 6, i.e. (a) 30 May, (b) 21 June, and (c) 18 July.

### 3.4 Deriving enthalpy of adsorption from the Halley field data

The enthalpies of adsorption between HNO<sub>3</sub>/ice and HO<sub>2</sub>NO<sub>2</sub>/ice have been derived in laboratory experiments carried out under environmentally relevant conditions. Ulrich et al. (2012) studied uptake of HO<sub>2</sub>NO<sub>2</sub> at low concentrations and temperatures between 230 and 253 K while Bartels-Rausch et al. (2002) and Ullerstam et al. (2005) studied the adsorption enthalpy of HNO<sub>3</sub>. Field studies carried out during the 24 h per day darkness of Antarctic winter provide optimum conditions for validating such laboratory-derived physical air/snow exchange parameters under “real-world” conditions.

At equilibrium, the partitioning of HO<sub>2</sub>NO<sub>2</sub> or HNO<sub>3</sub> molecules between the gas phase ( $C_g$ ) and the snow/ice sur-

**Table 2.** The enthalpies of adsorption to ice for HO<sub>2</sub>NO<sub>2</sub> and HNO<sub>3</sub> as derived from three periods of the Halley measurements. The number of observations used for each derivation is also given.

	HO <sub>2</sub> NO <sub>2</sub>		HNO <sub>3</sub>	
	$\Delta H_{\text{ads}}$ (kJ mol <sup>-1</sup> )	no. observations	$\Delta H_{\text{ads}}$ (kJ mol <sup>-1</sup> )	no. observations
30 May	-58 ± 2	144	-36 ± 2	144
21 June	-52 ± 2	90	-50 ± 2	82
18 July	-58 ± 2	55	-41 ± 4	55

face ( $C_s$ ) can be expressed as

$$K_{\text{part}} = \frac{C_s}{C_g}$$

As the partition constant will obey the van't Hoff equation, a new equation can be written as follows:

$$\frac{d \ln K_{\text{part}}}{d \frac{1}{T}} = -\frac{\Delta H_{\text{ads}}}{R},$$

where  $T$  is the temperature (K),  $\Delta H$  is the enthalpy of adsorption (J mol<sup>-1</sup>),  $R$  is the gas constant (8.314 J K<sup>-1</sup> mol<sup>-1</sup>).

Given our definition of  $K_{\text{part}}$  above, the equation can then be re-formulated as

$$\frac{d \ln \frac{C_s}{C_g}}{d \frac{1}{T}} = -\frac{\Delta H_{\text{ads}}}{R}.$$

At 240 K, roughly the temperatures of our observations, Ulrich et al. (2012), in their Fig. 4, show  $C_s / C_g \approx 20$  cm for HO<sub>2</sub>NO<sub>2</sub> and 8000 cm for HNO<sub>3</sub>. In the firn, the ratio of the surface area of snow to the volume of air is approximately 50 to 500 cm<sup>-1</sup> (based on a density of snow of 0.3 g cm<sup>-3</sup> and a specific surface area of 100 to 1000 cm<sup>2</sup> g<sup>-1</sup>; Domine et al., 2008). We can therefore calculate that the ratio of the number of molecules of HNO<sub>3</sub> adsorbed to the snow surface to that in the gas phase, is approximately  $4 \times 10^5$  to  $4 \times 10^6$ ; for HO<sub>2</sub>NO<sub>2</sub>, this ratio is 1000 to 10 000. As a result, for both HNO<sub>3</sub> and HO<sub>2</sub>NO<sub>2</sub>, exchange between the air and snow will thus have little effect on  $C_s$ , which can therefore be considered as a constant relative to  $C_g$ .

If we also assume that, over several hours, and under low and constant wind conditions, the concentration at our inlet tracks the concentration in the firn, then

$$\frac{d \ln C_g}{d \frac{1}{T}} = \frac{\Delta H_{\text{ads}}}{R}.$$

It is then possible to derive  $\Delta H_{\text{ads}}$  from the slope of  $\ln C_g$  vs.  $1/T$  multiplied by  $R$ .

For the Halley data, Fig. 7 shows plots of both  $\ln(\text{HNO}_3)$  vs.  $1/T$  and  $\ln(\text{HO}_2\text{NO}_2)$  vs.  $1/T$  for the time periods discussed in Sect. 3.3 above. As a reminder, these periods are

characterised by 24 h per day darkness, low wind speeds, and limited vertical mixing from turbulent diffusion, so are as close to laboratory conditions as could be found in our data set. They were also chosen as they spanned a reasonably large temperature range, which would improve the constraint on the linear fit.

The values of  $\Delta H_{\text{ads}}$  derived from these fits are given in Table 2. The average  $\Delta H_{\text{ads}}$  for HNO<sub>3</sub> is  $-42 \pm 2$  kJ mol<sup>-1</sup> which can be compared with laboratory-derived values of Bartels-Rausch et al. (2002) and Ullerstam et al. (2005). Bartels-Rausch et al. (2002) derived  $\Delta H_{\text{ads}}$  of  $-44$  kJ mol<sup>-1</sup> (with random error 2.3 kJ mol<sup>-1</sup>, systematic error 13 kJ mol<sup>-1</sup>); Ullerstam et al. (2005), working at lower concentrations of HNO<sub>3</sub>, relevant to the natural atmosphere, derived  $\Delta H_{\text{ads}}$  of  $-30.6 \pm 6.0$  kJ mol<sup>-1</sup>. For HO<sub>2</sub>NO<sub>2</sub>, the average  $\Delta H_{\text{ads}}$  derived from our field data is  $-56 \pm 1$  kJ mol<sup>-1</sup> which can be compared with the laboratory-derived value (Ulrich et al., 2012) of  $-59$  kJ mol<sup>-1</sup>. For both HO<sub>2</sub>NO<sub>2</sub> and HNO<sub>3</sub>, the agreement between laboratory and field-derived enthalpies of adsorption is remarkably good.

## 4 Summary and conclusions

We present the first high time resolution observations of HNO<sub>3</sub> and HO<sub>2</sub>NO<sub>2</sub> in coastal Antarctica, and the first from Antarctica during the dark winter period. Mixing ratios of HNO<sub>3</sub> ranged from instrumental detection limits to  $\sim 8$  parts per trillion by volume (pptv) and of HO<sub>2</sub>NO<sub>2</sub> varied from detection limits to  $\sim 5$  pptv. These values are on average lower than those observed at the South Pole in summer, where mixing ratios of HNO<sub>3</sub> and HO<sub>2</sub>NO<sub>2</sub> were generally in the 10s of pptv, and sometimes over 100 pptv.

The Antarctic, during winter, is an ideal natural laboratory for studying physical air/snow exchange processes. The environmental system is considerably simplified compared with other times of the year because of the lack of photochemical activity which must otherwise be taken into account when interpreting data.

In our study, we considered whether adsorption/desorption of HNO<sub>3</sub> and HO<sub>2</sub>NO<sub>2</sub> to snow/ice surfaces could be invoked to explain our observations; we did not consider formation of solid solutions from solid ice, or take-up to liquid

NaCl aerosols. In a follow-up study that further analysed our field data, Bartels-Rausch (2014) considered both the case of Langmuir adsorption to the ice surface, and solubility in ice forming a solid solution. He found that equilibrium air/snow partitioning was able to describe our field data well, both in terms of absolute mixing ratios and trend with temperature. He also found that the reservoir of adsorbed HNO<sub>3</sub> and HO<sub>2</sub>NO<sub>2</sub> in the upper snow pack was sufficient to fuel the observed emissions. In contrast, while calculations based on reversible solid-solution/air partitioning were able to describe mixing ratios of HNO<sub>3</sub>, they were not able to reproduce the observed trend with temperature. Further, the reservoir of HNO<sub>3</sub> in the outer part of the snow crystals was too small to explain observed increases in mixing ratio.

The measurements of HNO<sub>3</sub> and HO<sub>2</sub>NO<sub>2</sub> from Halley are consistent with laboratory experiments showing a temperature-dependence in the partitioning of both HNO<sub>3</sub> and HO<sub>2</sub>NO<sub>2</sub> to ice. They further support the conclusion that HO<sub>2</sub>NO<sub>2</sub>/ice interactions are stronger than those between HNO<sub>3</sub> and ice, as shown by the higher enthalpy of adsorption of HO<sub>2</sub>NO<sub>2</sub> compared with HNO<sub>3</sub> (Ulrich et al., 2012). On short timescales, therefore, HNO<sub>3</sub> and HO<sub>2</sub>NO<sub>2</sub> that is adsorbed to snow/ice can be re-released as temperatures rise. The snowpack can thus act as a source of HNO<sub>3</sub> and HO<sub>2</sub>NO<sub>2</sub> to the overlying atmosphere at all times of the year given sufficient reservoir in the snowpack and changing temperatures. Similarly, HNO<sub>3</sub> and HO<sub>2</sub>NO<sub>2</sub> adsorbed to cirrus clouds would be desorbed should temperatures rise. Such a reversible, temperature-dependent partitioning also provides a mechanism for re-distributing HNO<sub>3</sub> and HO<sub>2</sub>NO<sub>2</sub> on a local or regional scale across Antarctica. Snow can be transported considerable distances by storm systems, and adsorbed HO<sub>2</sub>NO<sub>2</sub> and HNO<sub>3</sub> can be desorbed as a function of changing temperature experienced along the transport pathway. Indeed, transport of snow from inland Antarctica is likely to contribute to the HO<sub>2</sub>NO<sub>2</sub> and HNO<sub>3</sub> reservoir in the coastal snowpack. The other likely source for HO<sub>2</sub>NO<sub>2</sub> to the winter snowpack is the general shift in equilibria, as temperatures fall from summer to winter, from gas-phase HO<sub>2</sub> and NO<sub>2</sub> towards gaseous HO<sub>2</sub>NO<sub>2</sub>, and then, by temperature-dependent partitioning, towards snowpack-adsorbed HO<sub>2</sub>NO<sub>2</sub>.

While clearly a controlling mechanism during polar night, the importance of air/snow partitioning relative to photochemistry will vary according to time of year and location. However, adsorption to/desorption from the snow pack should be taken into account when addressing budgets of boundary layer HO<sub>2</sub>NO<sub>2</sub> and HNO<sub>3</sub> at any snow-covered site, as all are likely to experience varying ambient temperature which would drive such air/snow exchange.

*Acknowledgements.* The authors thank Greg Huey and Dave Tanner for providing the CIMS instrument used in this work, and for their help in setting it up at Halley. A. E. Jones thanks Robert Mulvaney for useful discussions around this work. The authors are also grateful for Thorsten Bartels-Rausch for discussions and his subsequent modelling calculations. This study is part of the British Antarctic Survey Polar Science for Planet Earth Programme. It was funded by The Natural Environment Research Council (NERC).

Edited by: J. Roberts

## References

- Bartels-Rausch, T., Eichler, B., Zimmermann, P., Gaggeler, H. W., and Ammann, M.: The adsorption of nitrogen oxides on crystalline ice, *Atmos. Chem. Phys.*, 2, 235–247, doi:10.5194/acp-2-235-2002, 2002.
- Bartels-Rausch, T.: Ice-air partitioning of HNO<sub>3</sub> and HNO<sub>4</sub> drives winter mixing ratio, *Atmos. Chem. Phys. Discuss.*, 14, C4673–C4694, 014.
- Bauguitte, S. J.-B., Bloss, W. J., Evans, M. J., Salmon, R. A., Anderson, P. S., Jones, A. E., Lee, J. D., Saiz-Lopez, A., Roscoe, H. K., Wolff, E. W., and Plane, J. M. C.: Summertime NO<sub>x</sub> measurements during the CHABLIS campaign: can source and sink estimates unravel observed diurnal cycles?, *Atmos. Chem. Phys.*, 12, 989–1002, doi:10.5194/acp-12-989-2012, 2012.
- Buys, Z., Brough, N., Huey, L. G., Tanner, D. J., von Glasow, R., and Jones, A. E.: High temporal resolution Br<sub>2</sub>, BrCl and BrO observations in coastal Antarctica, *Atmos. Chem. Phys.*, 13, 1329–1343, doi:10.5194/acp-13-1329-2013, 2013.
- Chen, G., Davis, D., Crawford, J., Nowak, J. B., Eisele, F., Mauldin, R. L., Tanner, D., Buhr, M., Shetter, R., Lefter, B., Arimoto, R., Hogan, A., and Blake, D.: An investigation of South Pole HO<sub>x</sub> chemistry: Comparison of model results with ISCAT observations, *Geophys. Res. Lett.*, 28, 3633–3636, 2001.
- Cotter, E. S. N., Jones, A. E., Wolff, E. W., and Bauguitte, S. J.-B.: What controls photochemical NO and NO<sub>2</sub> production from Antarctic snow? Laboratory investigation assessing the wavelength and temperature dependence, *J. Geophys. Res.*, 108, 4147, doi:10.1029/2002JD002602, 2003.
- Davis, D., Nowak, J. B., Chen, G., Buhr, M., Arimoto, R., Hogan, A., Eisele, F., Mauldin, L., Tanner, D., Shetter, R., Lefter, B., and McMurtry, P.: Unexpected high levels of NO observed at South Pole, *Geophys. Res. Lett.*, 28, 3625–3628, 2001.
- Davis, D., Chen, G., Buhr, M., Crawford, J., Lenschow, D., Lefter, B., Shetter, R., Eisele, F., Mauldin, L., and Hogan, A.: South Pole NO<sub>x</sub> chemistry: an assessment of factors controlling variability and absolute levels, *Atmos. Environ.*, 38, 5375–5388, 2004.
- Davis, D. D., Seelig, J., Huey, G., Crawford, J., Chen, G., Wang, Y., Buhr, M., Helmig, D., Neff, W., Blake, D., Arimoto, R., and Eisele, F.: A reassessment of Antarctic plateau reactive nitrogen based on ANTICI 2003 airborne and ground based measurements, *Atmos. Environ.*, 42, 2831–2848, doi:10.1016/j.atmosenv.2007.07.039, 2008.
- Domine, F., Albert, M., Huthwelker, T., Jacobi, H.-W., Kokhanovsky, A. A., Lehning, M., Picard, G., and Simpson, W. R.: Snow physics as relevant to snow photochemistry, *Atmos. Chem. Phys.*, 8, 171–208, doi:10.5194/acp-8-171-2008, 2008.



- Eisele, F., Davis, D., Helmig, D., Oltmans, S., Neff, W., Huey, G., Tanner, D., Chen, G., Crawford, J., Arimoto, R., Buhr, M., Mauldin, L., Hutterli, M., Dibb, J., Blake, D., Brooks, S.B., Johnson, B., Roberts, J., Wang, Y., Tan, D., and Flocke, F.: Antarctic tropospheric chemistry investigation (ANTCI) 2003 overview, *Atmos. Environ.*, 42, 2749–2761, doi:10.1016/j.atmosenv.2007.04.013, 2008.
- Hudson, P. K., Shilling, J. E., Tolbert, M. A., and Toon, O. B.: Uptake of nitric acid on ice at tropospheric temperatures: Implications for cirrus clouds, *J. Phys. Chem. A*, 106, 9874–9882, 2002.
- Huey, L. G., Tanner, D. J., Slusher, D. L., Dibb, J. E., Arimoto, R., Chen, G., Davis, D., Buhr, M. P., Nowak, J. B., Mauldin, R. L., Eisele, F. L., and Kosciuch, E.: CIMS measurements of HNO<sub>3</sub> and SO<sub>2</sub> at the South Pole during ISCAT 2000, *Atmos. Environ.*, 38, 5411–5421, 2004.
- Huthwelker, T., Ammann, M., and Peter, T.: The uptake of acidic gases on ice, *Chem. Rev.*, 106, 1375–1444, 2006.
- Jones, A. E., Wolff, E. W., Salmon, R. A., Bauguutte, S. J.-B., Roscoe, H. K., Anderson, P. S., Ames, D., Clemitchaw, K. C., Fleming, Z. L., Bloss, W. J., Heard, D. E., Lee, J. D., Read, K. A., Hamer, P., Shallcross, D. E., Jackson, A. V., Walker, S. L., Lewis, A. C., Mills, G. P., Plane, J. M. C., Saiz-Lopez, A., Sturges, W. T., and Worton, D. R.: Chemistry of the Antarctic Boundary Layer and the Interface with Snow: an overview of the CHABLIS campaign, *Atmos. Chem. Phys.*, 8, 3789–3803, doi:10.5194/acp-8-3789-2008, 2008.
- Kim, S., Huey, L. G., Stickel, R. E., Tanner, D. J., Crawford, J. H., Olson, J. R., Chen, G., Brune, W. H., Ren, X., Leshner, R., Wooldridge, P. J., Bertram, T. H., Perring, A., Cohen, R. C., Lefer, B. L., Shetter, R. E., Avery, M., Diskin, G., and Sokolik, I.: Measurement of HO<sub>2</sub>NO<sub>2</sub> in the free troposphere during the intercontinental chemical transport experiment – North America 2004, *J. Geophys. Res.-Atmos.*, 112, D12S01, doi:10.1029/2006JD007676, 2007.
- Neuman, J. A., Huey, L. G., Ryerson, T. B., and Fahey, D. W.: Study of inlet materials for sampling atmospheric nitric acid, *Environ. Sci. Technol.*, 33, 1133–1136, doi:10.1021/es980767f, 1999.
- Popp, P. J., Gao, R. S., Marcy, T. P., Fahey, D. W., Hudson, P. K., Thompson, T. L., Karcher, B., Ridley, B. A., Weinheimer, A. J., Knapp, D. J., Montzka, D. D., Baumgardner, D., Garrett, T. J., Weinstock, E. M., Smith, J. B., Sayres, D. S., Pittman, J. V., Dhaniyala, S., Bui, T. P., and Mahoney, M. J.: Nitric acid uptake on subtropical cirrus cloud particles, *J. Geophys. Res.*, 109, D06302, doi:10.1029/2003JD004255, 2004.
- Slusher, D. L., Pitteri, S. J., Haman, B. J., Tanner, D. J., and Huey, L. G.: A chemical ionization technique for measurement of pernitric acid in the upper troposphere and the polar boundary layer, *Geophys. Res. Lett.*, 28, 3875–3878, doi:10.1029/2001GL013443, 2001.
- Slusher, D. L., Huey, L. G., Tanner, D. J., Chen, G., Davis, D. D., Buhr, M., Nowak, J. B., Eisele, F. L., Kosciuch, E., Mauldin, R. L., Lefer, B. L., Shetter, R. E., and Dibb, J. E.: Measurements of pernitric acid at the South Pole during ISCAT 2000, *Geophys. Res. Lett.*, 29, 2011, doi:10.1029/2002GL015703, 2002.
- Slusher, D. L., Neff, W. D., Kim, S., Huey, L. G., Wang, Y., Zeng, T., Tanner, D. J., Blake, D. R., Beyersdorf, A., Lefer, B. L., Crawford, J. H., Eisele, F. L., Mauldin, R. L., Kosciuch, E., Buhr, M. P., Wallace, H. W., and Davis, D. D.: Atmospheric chemistry results from the ANTCI 2005 Antarctic plateau airborne study, *J. Geophys. Res.-Atmos.*, 115, D07304, doi:10.1029/2009JD012605, 2010.
- Stull, R. B.: *An Introduction to Boundary Layer Meteorology*, Kluwer Academic Publishers, Dordrecht, 670 pp., 1988.
- Ullerstam, M., Thornberry, T., and Jonathan, P. D., and Abbatt, J. P. D.: Uptake of gas-phase nitric acid to ice at low partial pressures: evidence for unsaturated surface coverage, *Faraday Discuss.*, 130, 211–226, doi:10.1039/B417418F, 2005.
- Ulrich, T., Ammann, M., Leutwyler, S., and Bartels-Rausch, T.: The adsorption of peroxyxynitric acid on ice between 230 K and 253 K, *Atmos. Chem. Phys.*, 12, 1833–1845, doi:10.5194/acp-12-1833-2012, 2012.
- Weinheimer, A. J., Campos, T. L., Walega, J. G., Grahek, F. E., Ridley, B. A., Baumgardner, D., Twohy, C., and Gandrud, B.: Uptake of NO<sub>y</sub> on wave-cloud ice particles, *Geophys. Res. Lett.*, 25, 1725–1728, 1998.
- Ziereis, H., Minikin, A., Schlager, H., Gayet, J. F., Auriol, F., Stock, P., Baehr, J., Petzold, A., Schumann, U., Weinheimer, A., Ridley, B., and Strom, J.: Uptake of reactive nitrogen on cirrus cloud particles during INCA, *Geophys. Res. Lett.*, 31, L05115, doi:10.1029/2003GL018794, 2004.